3 Sensors

This chapter introduces sensors often usedcome on autonomous mobile vehicles. In general, a sensor or a sensor system transforms different kinds of physical values (e. g. a force or a velocity) into electrical signals. One can distinguish sensors according to the integration level (see also figure 3.1):

Basic sensor: measurement and transformation of the physical signals,

Integrated sensor: basic sensor with signal processing including amplification, filtering, linearization and normalization,

Intelligent sensor: integrated sensor with computer-controlled analysis of the processed signal.

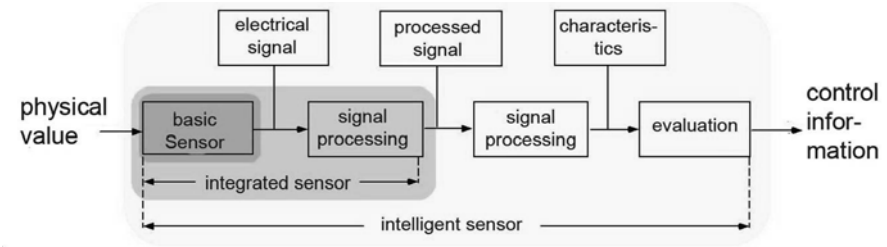

Figure 3.1 Sensor integration levels

Another way of classifying sensors often used in literature is the separation into proprioceptive sensors and exteroceptive sensors. Proprioceptive sensors measure internal states of a robot (e. g. wheel velocity or acceleration), while exteroceptive sensors observe the state of the robot in relation to its environment (e. g. distance to an obstacle or object identification).

On the other hand, one can also distinguish between active and passive sensors. Active sensors stimulate the environment and analyze the responding signal (e. g. ultrasound sensors, laser scanners) while passive sensors measure a present signal (camera, microphone).

All sensors share an inability to measure their respective variable perfectly. There always is a measurement error, depending on the measurement principle.

In the following, sensors that are useful for autonomous land vehicles are summarized according to perception characteristics and operating principles. It makes no sense to describe specific products on the market in this section, since they change continuously.

3.1 Tactile sensors

Tactile sensors detect physical contact between the vehicle and an obstacle. This type of sensor is often used in simple mobile robots as a cheap possibility to describe the environment of the robot. On the other hand, tactile sensors are often used to fulfill safety requirements imposed on a robot: physical contact of the vehicle with an obstacle causes an emergency stop.

3.1.1 Switches

Operated by a force larger than a defined minimal force, a spring loaded contact, which closes or opens an electric circuit, induces a signal. This might be used to detect more than an unwanted contact with the environment.

3.1.2 Bumper

As a last resort before crashing into an obstacle a bumper activates an emergency break and consumes some part of the impulse like passive bumpers on cars. This is done by a more or less elastic shield, fastened by springs to the vehicle chassis. Switches detect the deformation of the shield (see figure 3.2).

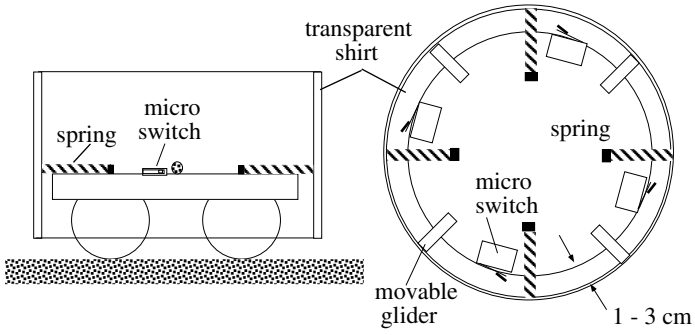

Figure 3.2 Sketch of a simple bumper fixed to the robot chassis (sideview and bird's eye view)

3.1.3 Force sensors

Typically, force sensors use the physical deformation of elastic materials. This deformation changes properties of the material like electrical resistance or capacity. The parameters of a force sensor are the minimal detectable force, the maximal allowed force and the speed at which a changing force can be measured. In wheel-driven vehicles, force sensors fixed on the wheels are often used to prevent tilting over. Also slipping of the vehicle can be detected with the help of force sensors.

For example, the climbing robot CROMSCI of the University of Kaiserslautern possesses 3 steerable wheels. In each wheel a 3-component force sensor is integrated which measures contact forces in x-, y-, and z-direction, see figure 3.3 and 3.4. The maximum forces in x- and y-direction are 150 N while in z-direction 1500 N could be detected with a resolution of 1 N.

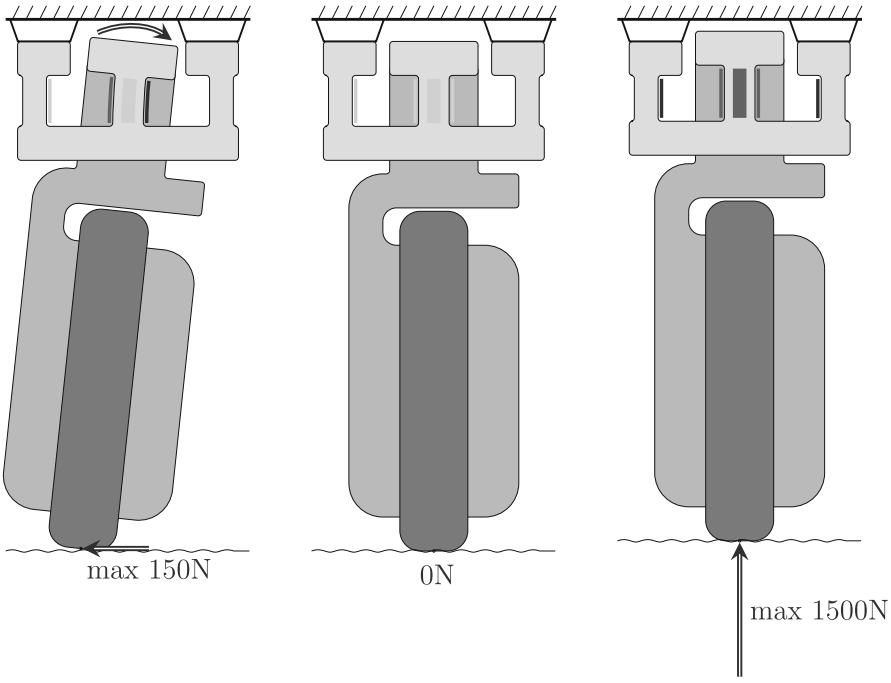

Figure 3.3 Measurement principle of wheel-mounted force sensors. Strain gages are glued to specific parts of the sensor box. The forces in the wheels lead to a deformation of these parts which cause a change in the resistance of the strain gages. The measured fall of voltage is proportional to the change of forces.

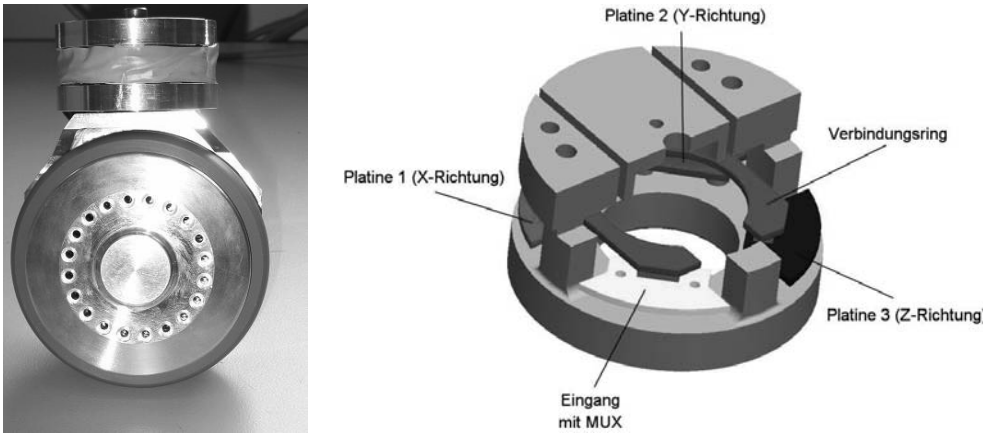

Figure 3.4 The driven wheel of CROMSCI equipped with a force sensor (left) and the force sensor with integrated electronics (right)

3.2 Pose measurement

The pose of a vehicle is its position and orientation with respect to a world coordinate system. There are different possibilities to determine this pose. Most techniques are based on odometry sensors, landmarks, magnetic compasses or inclinometers. The sensors which belong to these classes have in common that they are not precise enough to solve the pose estimation problem independently. In chapter 4, some methods of improving postion estimates are shown.

3.2.1 Odometry sensors

A robot's trajectory derived from the summation of wheel speeds is called odometry. However without orientation sensor, this odometry works only in 2D.

Wheel encoders are mainly used for the determination of the wheel speed. Based on the measurement principle one can discern magnetic and optical wheel encoders. Magnetic wheel encoders measure the number of magnetic pole changes of magnets at the perimeter of a disk either by hall effect sensors or by the voltage produced by an electric generator turned by the wheel (tacho generator).

Optical wheel encoders measure distances by the number of ticks produced by a grid passing a light barrier. There are two grids: one fixed to the vehicle chassis, the other one turning with the wheel. Hence, the movement

of the vehicle might be tracked simply counting the number of ticks at the wheels resulting in the distance travelled.

Let n be the number of ticks measured and n_0 the number of ticks for a full revolution of the wheel with radius r. The distance travelled then is $s = 2\pi r \cdot \frac{n}{n_0}$.

As presented in figure 3.5, the encoder is also capable of measuring the direction of the rolling wheel. Two grids, fixed to the vehicle chassis $\left(\left(\frac{n+1}{4}\right)\right)$ grid constants apart, emit two signals with a phase difference of 90° from which the direction may be derived. Typical wheel encoders have grids of 4096 equidistant transparent and nontransparent areas. These encoders have a resolution of 12 Bit or 0.1°. The calculations towards the vehicle pose are to be found in chapter 4.

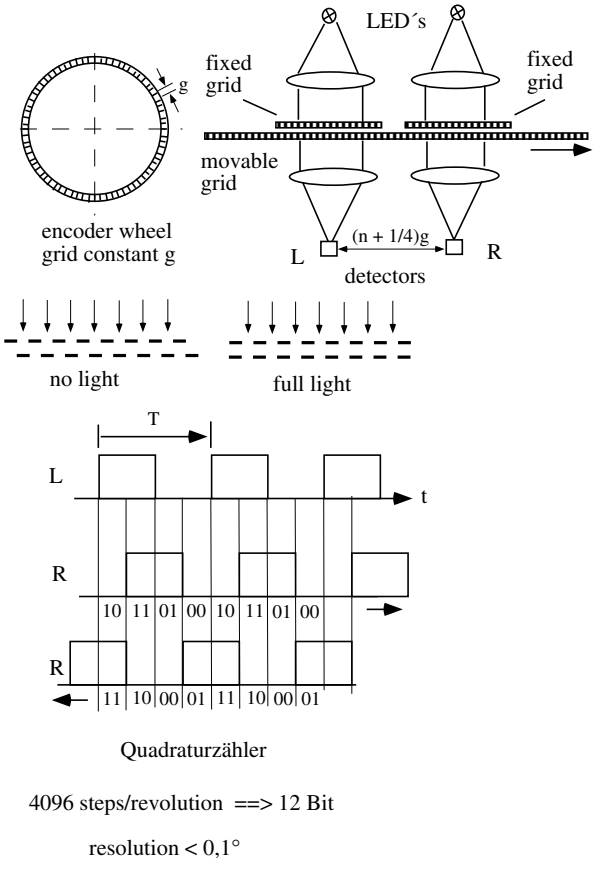

Figure 3.5 Measurement principle of a wheel-encoder

3.2.2 Compass

A magnetic compass can be used to keep a direction, measuring the horizontal component of the earth's magnetic field assumed to be constant in its direction over short distances. Apart from the classical compass as used on ships for hundreds of years, this can be done using a ferrite slab with a rectangular hysteresis loop. Any external magnetic field in the long direction of the slab shifts the magnetization where the slab goes into saturation.

In a coil wound around the slab driven by a varying current the point of saturation shows up in a voltage peak induced in the coil by the sudden change of magnetization. Driving the coil with a time varying current ramp, the hysteresis loop is scanned periodically. The component of the field in the direction of the slab can thus be measured as shown in figure 3.6. Two crossed slabs give the direction of the earth's magnetic field as seen from the vehicle. In indoor applications, the magnetic field in the room is mostly disturbed by metallic parts in concrete walls and ceilings.

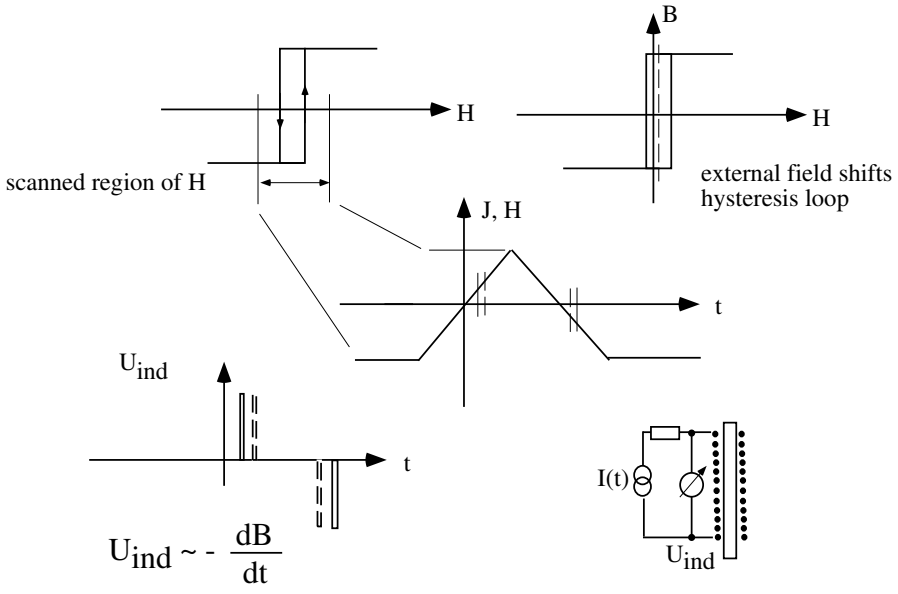

Figure 3.6 Principle of the flux-gate sensor

3.2.3 Inclinometers

In order to measure whether an autonomous vehicle moves up or down a steep incline or shifts to a side, with the danger of toppling or falling to the

side, the inclination must be measurable in two axes. This can be done using a droplet of liquid under the influence of gravity as shown in figure 3.7. In a transparent hemispherical plastic bowl filled with oil, a droplet of water forms a lens at the bottom, because water is more dense than oil. The light of a LED is projected by that lens onto a CCD-matrix. Any inclination shifts the droplet and so the image of the LED on the CCD-matrix, indicating the amount of inclination. An oil of suitable viscosity damps the movement of the water droplet to damp jitter from movements over uneven ground.

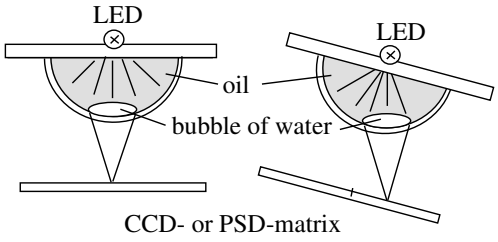

Figure 3.7 Measuring principle of an optical inclinometer

Figure 3.8 shows the principle of another device; a dielectric liquid drop floats between the plates of a capacitance. Any tilt shifts the drop to the side and changes the capacitances in a quad capacitance measuring device. Typical parameters for a specific sensor of this type are also shown.[1]

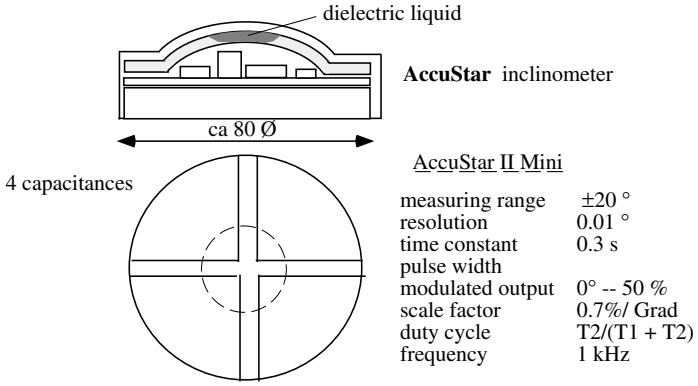

Figure 3.8 Measurement principle of a capacitive inclinometer

[1] Althen GmbH, Frankfurterstr. 150–152, D65779 Kelkheim, Germany; `http://www.althen.de/neigungssensoren`

3.3 Sensors for inertial systems

Determining the pose of a vehicle may be done by measuring only accelerations and turning rates and integrating these signals. These measurements are independent from any disturbances of the outside world.

3.3.1 Acceleration sensors

Accelerometers measure the component of the acceleration in one direction.

Apart from a crash the accelerations in a vehicle driving around are in general a lot smaller than the earth acceleration of 1 g.

Driving through a curve in a car will result in accelerations in the magnitude of approximately 0.1 g. Measuring devices found in an airbag system can also be used for autonomous vehicles.

An example is the AD-XL 105 by Analog Devices.[2] It is a device fabricated as a MEMS, a micro electro-mechanical system, etched out of silicon and housed in a 14 pin DIP (dual inline package) like a small integrated circuit.

Its parameters are

AD XL 105	
measuring range	$\pm$ 5 g
smallest detectable acceleration	0.02 g
operating voltage	5 V
output	0.25 V/g (analog)
bandwidth	10 kHz

The device includes an uncommitted amplifier to amplify the output A by the quotient of two external resistors: output $= (R_1/R_2) \cdot A \cdot 0.25\,\mathrm{V/g}$ with acceleration A.

There are other sensors available that can measure more than one axis at the same time. An example for such a sensor is presented in figure 3.9. The AD-XL 202 is a two axis system by Analog Devices housed in a 14 pin DIP with parameters

AD XL 202	
measuring range	$\pm$5 g
smallest detectable acceleration	0.01 g

[2] `http://www.analog.com/en/mems-and-sensors/imems-accelerometers/`

operating voltage	5 V
output	2 PWM TTL signals
pulse period	1–10 ms
measured acceleration A	$A = \frac{(T_2/T_1)-0.5}{12.5}$

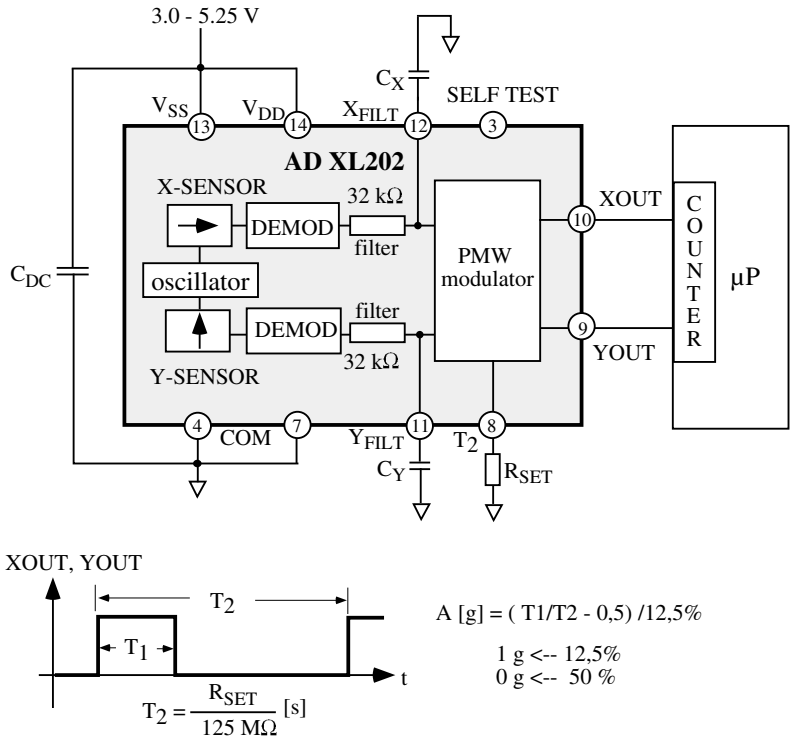

Figure 3.9 Two axis accelerometer AD XL 202

The pulse width is externally adjustable with 1 g equalling 12,5% and 0 g equalling 50%. Two built in filters at the output of the demodulator integrate the measured different signals. The integration time constant is set with the capacitors C_x and C_y. The period of the pulse width modulator at the output is set by resistor R_{SET}. Figure 3.10 shows a MEMS-version of this accelerometer.

Nowadays, usually micro electro-mechanical systems (MEMS) are used. They integrate complex electro-mechanical systems into bulk silicon. Silicon is a material with good properties for this type of application and it is very well understood in its physical and crystallographic properties from decades of producing integrated circuits. The same technique that is used to form

ICs may also be applied to etch out free swinging beams of silicon anchored to the bulk material at a few points only.

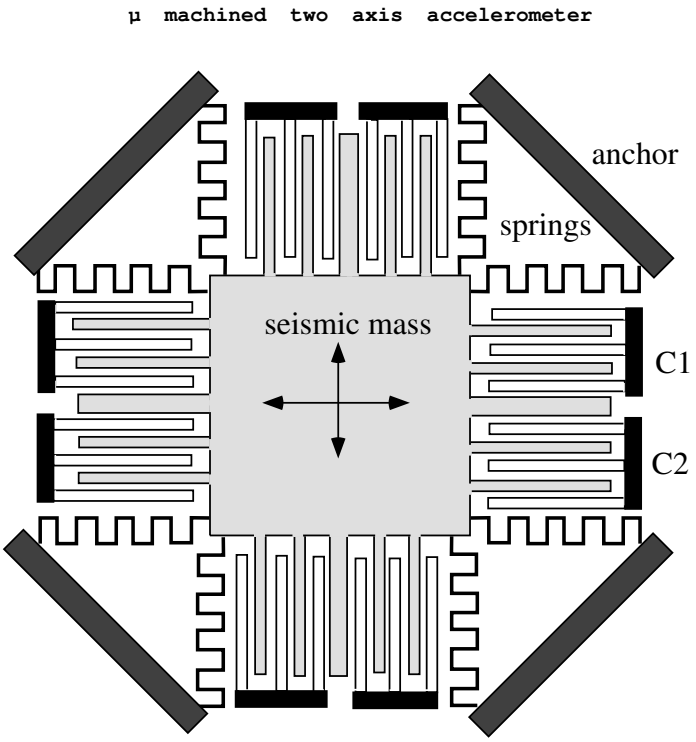

Example: Analog Devices AD XL 202

measuring range	± 2 g
smallest detectable acceleration	1 mg
operating voltage	5 V
housing	14 DIP
output	2 PWM TTL signals
pulse period	1-10 ms externally adjustable

Figure 3.10 Two axis accelerometer

The measurement principle here is a pair of capacitors to measure very small distance variations under acceleration. A central difficulty with acceleration sensors is given by earth acceleration which in most cases is far larger than the acceleration of the vehicle to be measured. Therefore, the orientation information is crucial to remove unwanted gravity forces from the measurement results.

Figure 3.11 depicts the principle. A mass anchored to the bulk by plate springs is forced into oscillations by a comb of slabs acting as capacitors. Typical dimensions of the slabs are length $s = 125\,\mu$m, thickness $b = 1\,\mu$m and distance to the next slab $d = 1\,\mu$m. The force is multiplied by the number of combs gripping into each other. It acts in one direction only, but activating two combs at each side of the masses by alternatively switching the voltage driving the combs will set the system into oscillations. Typical frequencies are in the order of approx. 20 kHz. The forces are small, but as the damping of the system is very small, they are sufficient to drive the block into oscillations with voltages of 5 V.

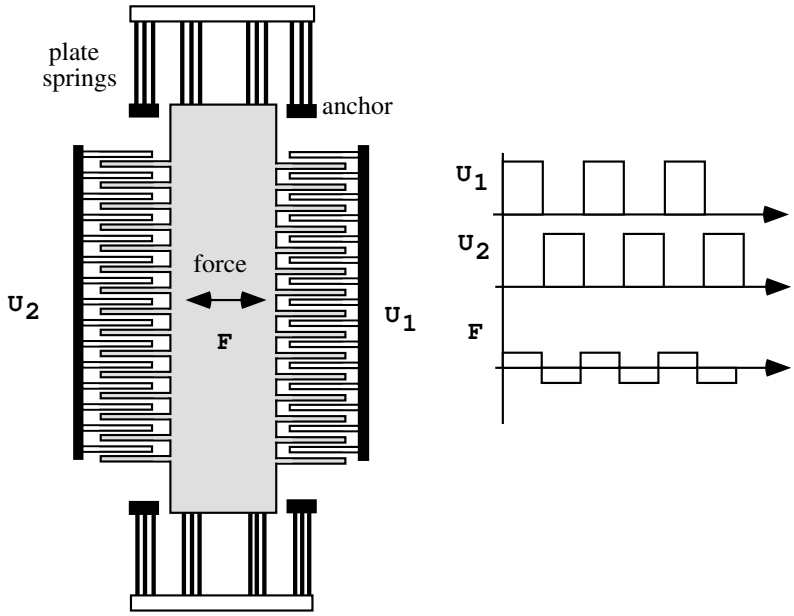

Figure 3.11 Forced oscillations

To measure small deviations down to 1 nm the slabs may be used as differential capacitors as shown in figure 3.12.

Driving the capacitors by two voltages with 180° phase shift, the resulting signal after synchronous demodulation is proportional to the difference in capacitances and measures the deviation Δd. Since the measuring frequency is much larger than the frequency driving the oscillation they do not interfere with each other.

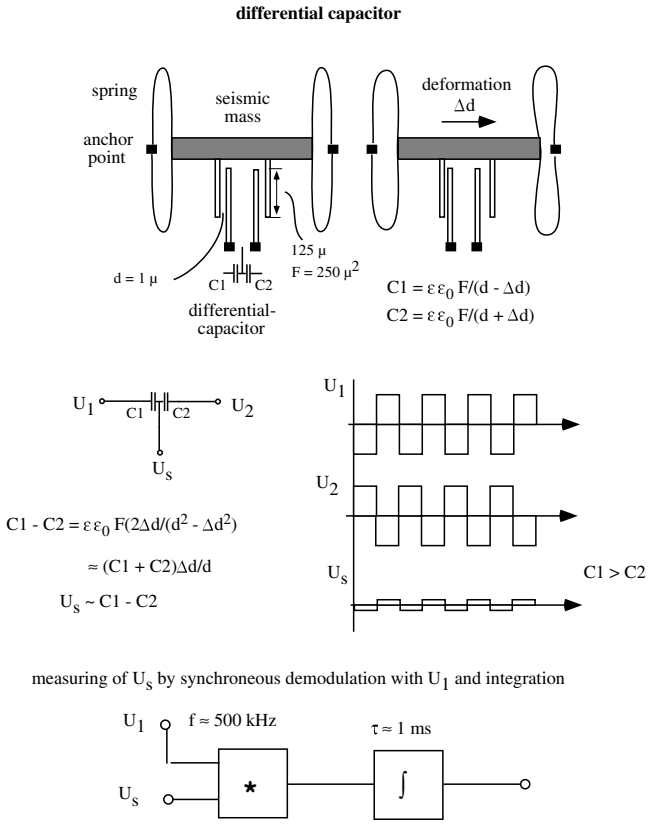

Figure 3.12 Differential capacitor

3.3.2 Turning rate sensors

Angular velocity sensors are intended to measure the turning rate of the vehicle. Their precision need not be too high: it is neither necessary to see the rotation of the earth with 15°/h at a pole, nor the slow rotation of the short arm of a clock of 30°/h or 0,008°/s if the position and orientation has to be kept for minutes only until the vehicle can reorient itself from landmarks again.

Cheap sensors for this application are again MEMS devices. Figure 3.13 shows such a sensor. Two seismic masses are forced into oscillations by comb drivers, operating 180° out of phase. Inside each mass a measuring comb forming the differential capacitors C_a, C_b, C_c and C_d respectively measure any deviation due to the Coriolis force and the amplitude of the driving oscillation.

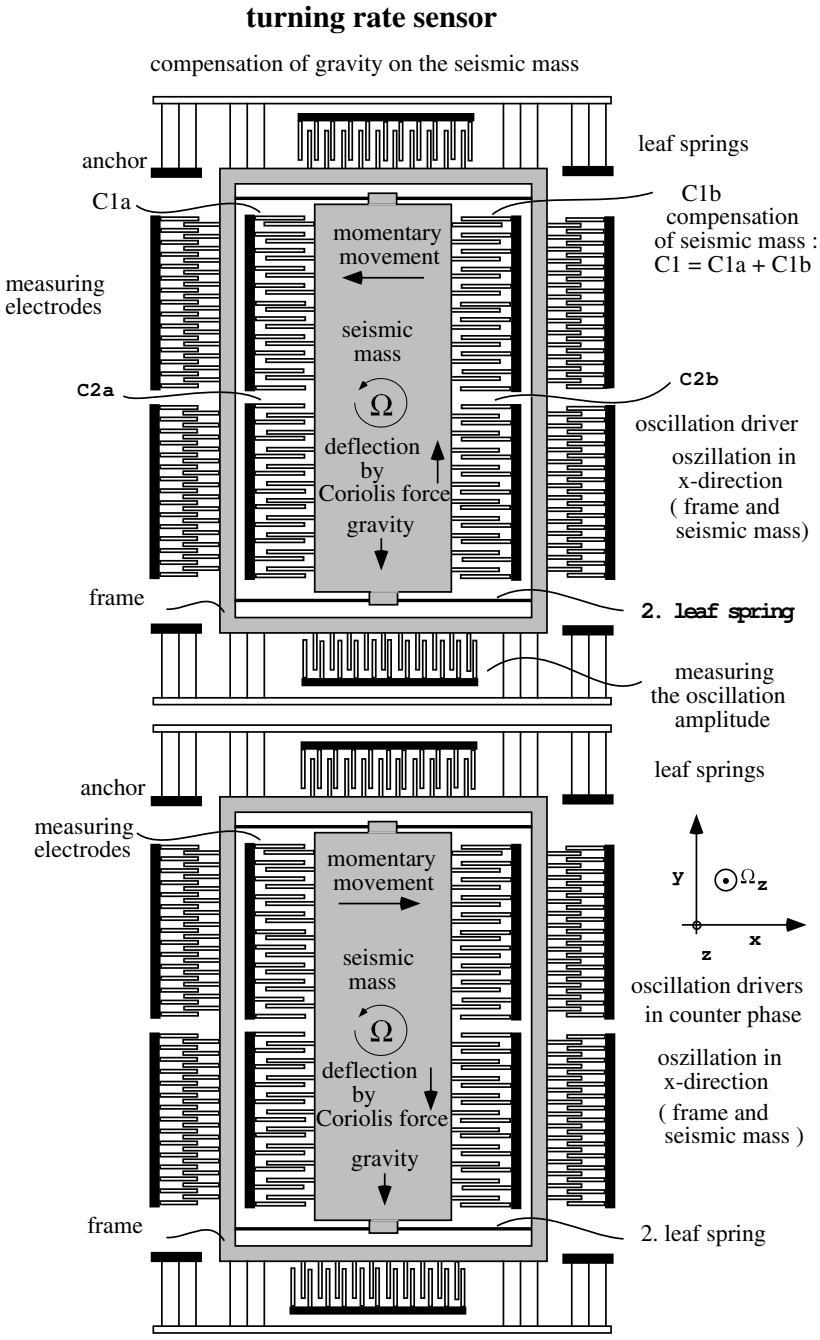

Figure 3.13 Turning rate sensor

The amplitude of the driving oscillation is $A\omega \sin \omega t$ using the differential capacitors as $(C_a + C_c) - (C_b + C_d)$, while the amplitude of the turning rate Ω is measured through $\Omega A\omega \sin \omega t$ using $(C_a + C_b) - (C_c + C_d)$ in a synchronous detector.

An example of a turning rate sensor is ADXRS150 from Analog-Devices.[3]

ADXRS150

measuring range	$\pm 150°/s$ i. e. $\pm 2{,}62$ rad/s
non linearity	0,1%
acceleration influence	0.023°/s/g
temperature influence	15% or 21.7°/s(−40° C to +85°C), $0.17°/s/°$C

The latest MEMS devices include 3-axis accelerometers with dimensions of 4 mm × 4 mm × 1.45 mm in a 16-pin plastic lead frame chip scale package (LFCSP) as for instance the ADXL330 from Analog Devices. It offers a measuring range of ±3 g and a sensitivity of 300 mV/g. Packing a three-axis accelerometer and three turning rate sensors into one package gives a six-axis movement sensor, the ADIS16355 from Analog Devices.

In order to find the position and orientation of a vehicle without reference to external landmarks there must be precise sensors on board to measure the turning of the vehicle using inherent physical properties. If the position and orientation have to be maintained for longer times, the turning rate sensors must be precise – and consequently be expensive.

Laser Gyros use the so-called Sagnac effect. It exploits the fact that the speed of light stays constant regardless of the velocity of the sender. In a material with the refractive index $n(\lambda)$ and the speed of light in vacuum c_0, light travels at a velocity of $c = c_0/n(\lambda)$ irrespective of the velocity of the material itself. A comparatively cheap measuring device based on this effect is a laser fiber coil gyro.

Two light beams run in opposite directions in a fiber coil: one clockwise the other one counterclockwise. If the coil itself turns, a phase shift between entrance and exit of $\varphi = 2\omega LD/(\lambda c)$ will occur with L being the fiber length, D the diameter and ω the turning rate of the coil. Figure 3.14 illustrates the principle.

The system's specifications are:

Hitachi Optical Fiber Gyroscope

maximum input rotation rate	$\pm 100°/s$
minimum detectable rotation rate	$\pm 0{,}01°/s$
zero point drift	$\leq 10°/h$

[3] `http://www.analog.com/en/mems-and-sensors/imems-gyroscopes/`

dimensions	100 mm×100 mm×60 mm
weight	0.5 kg
analog output	$\pm 2.5V$ at 350 mA
digital output	TTL, 9600 Bit/s
answer time	10 ms
warm up time	$\leq$1 min

A zero point drift of $10°/h$ is just the rotation of the earth at 40° latitude. A rotation rate of $0.01°/s$ equals $36°/h$ and is enough to detect the earth rotation. In order to derive the turning angle the signal from the rate sensor has to be integrated:

$$\psi(t) = \int_0^t \omega(\tau) d\tau \tag{3.1}$$

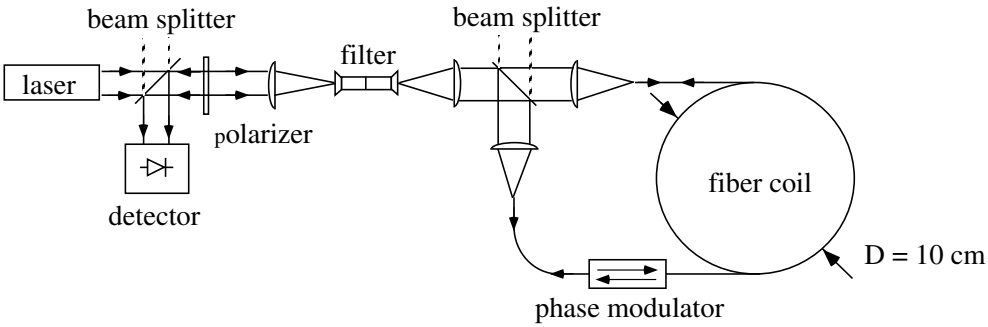

Figure 3.14 Principle of Hitachi Fiber Coil Gyro

Mechanical Gyros make use of the fact that a system with a constant angular momentum isolated from external torques keeps its angular momentum and thus its direction.

A torque $\vec{D}$ acting upon a system with angular momentum $\vec{J}$ induces a precession ω_p with $\vec{J}\omega_p = \vec{D}$ in the system.

Its direction is perpendicular to the plane spanned by $\vec{D}$ and $\vec{J}$.

Its magnitude is the product of the magnitudes of $\vec{D}$ and $\vec{J}$ and the sinus of the included angle γ as shown in figure 3.15 – the cross-product of the vectors of torque and angular momentum.

This is directly exploited in mechanical gyros – costly but precise. For autonomous vehicles, maintaining a desired direction is necessary for rather short periods only when there is no external reference available. In this case turning rate sensors based on the Coriolis force may be used: A swinging

mass represents an angular momentum too and a forced precession ω_p is translated into a force F perpendicular to the swinging motion and the forced precession, as shown in the same figure as above and exploited in MEMS turning rate sensors described above.

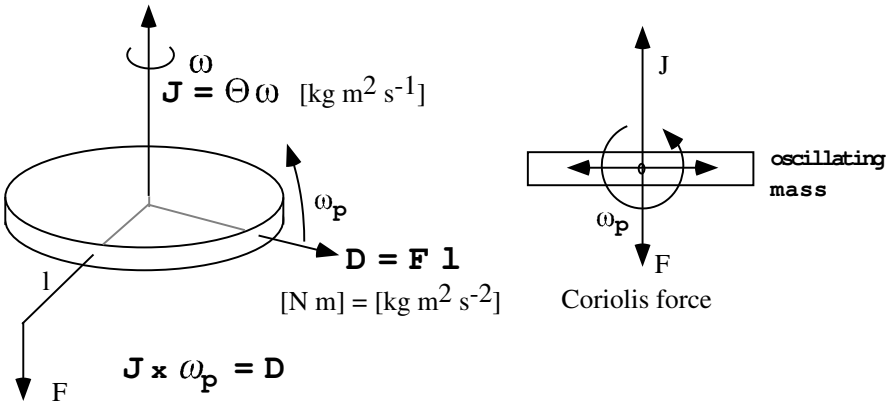

Figure 3.15 Precession and Coriolis force

Murata Gyro Star[4] An explicit Coriolis force based sensor is built around a triangular quartz prism set into vibrations like a quartz slab in an electronic clock. Any turning along the main axis causes the prism to swing in other directions as well.

Two electrodes measure these vibrations. Their signal is proportional to the turning rate as shown in figure 3.16.

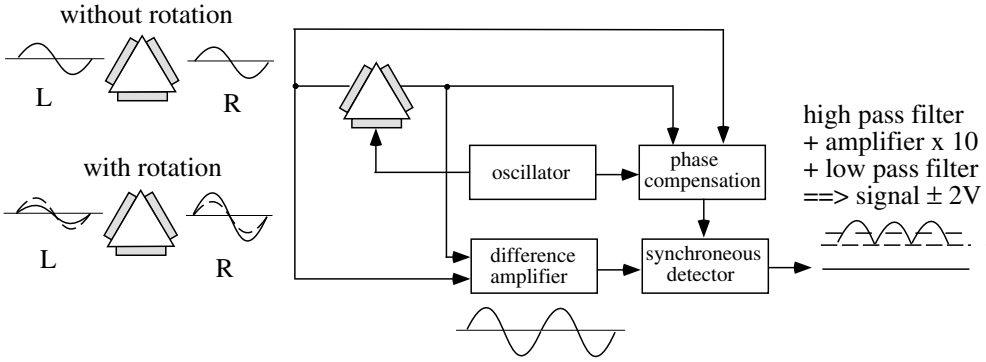

Figure 3.16 Principle of the Murata gyro compass

[4] http://www.murata.com/catalog/s42e.pdf

Typical specifications are listed below:

Murata Gyrostar EBNC o3J	
external voltage	[+2.7V, + 5.5V]
current	5 mA
max. angular velocity	±300°/s
output at $\omega = 0$	+ 1.35 V
scale factor	0,67 $\frac{\text{mV}}{\circ/\text{s}}$
temperature coefficient	±20%
linearity	±0,5% of maximum signal
dimensions	15.5 mm×8.0 mm×4.3 mm
measuring rate	50 Hz maximum
weight	1.0 g

3.4 Distance sensors

Distance or proximity sensors are crucial for autonomous vehicles regarding collision avoidance and mapping. Distance sensors can be active or passive. Besides passive camera systems, there are active systems based on measurement principles like ultrasonic, infrared or lasers, see figure 3.17.

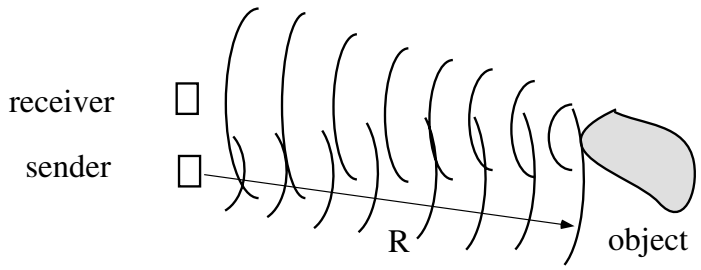

Figure 3.17 An active distance measuring system

For this kind of sensors the energy taken up at the site of the sensor depends on

- the sensing surface B of the receiver,
- the surface A of the object hit by the beam,
- the reflection $\rho(\alpha)$ of the beam from the object, being dependent on the angle of incidence to the surface normal and the reflectivity ($\geq$ 99% for mirrors down to 0,01% for strong absorbing surfaces like black soot).

The light intensity at the object $f(R)$ depends on the type of light source:

- $f(R) = \alpha = const$ for a laser beam hitting the object fully.
- $f(R) = a/R^2$ for other light sources with large radiation cones compared to the object,
- $f(R) = e^{-R/\gamma} \cdot a/R^2$ holds true if the light is being absorbed in the medium like e. g. light in fog or ultra sound in air.

At the object the reflected signal is $I_1 = A \cdot \rho(\alpha) \cdot I(R)$ with A the surface of the object for a normal source or surface of the laser beam with diameter Φ if the surface of the object is larger than $\pi/4 \cdot \Phi^2$.

$\rho(\alpha)$ is the reflectivity depending on impact angle α. At the site of the detector, the intensity is $I(D) = I_1 \cdot f_2(R) \cdot B$ with $f_2(R) = b/R^2$, b the proportion cut out of the reflected beam by the detector, and B the surface of the detector. Together this can be summarized to

$$I(D) = A \cdot I_0 \cdot \rho(\alpha) \cdot f(R) \cdot f_2(R) \cdot B \tag{3.2}$$

$$\boxed{I(D) = A \cdot B \cdot 1/R^4 \cdot I_0 \cdot \rho(\alpha) \cdot a \cdot b} \tag{3.3}$$

This is the **Radar equation** without a laser and without absorption. Note the strong dependency on the distance with the inverse fourth power in R. Using a laser beam with a surface area of $\pi/4 \cdot \Phi^2$ the radar equation becomes

$$I(D) = \pi/4 \cdot \Phi^2 \cdot B \cdot 1/R^2 \cdot I_0 \cdot \rho(\alpha) \cdot a \cdot b \tag{3.4}$$

The advantage of using a sharply bundled illuminating source like a laser beam is the reduced dependency on R:
$I(D) \propto R^{-4} \longrightarrow I(D) \propto R^{-2}$.

In the following text different types of distance sensor for which the radar equation can be used are presented.

3.4.1 Infrared sensors

Distance measurement with infrared light is typically used as proximity sensors to detect nearby obstacles (5–80 cm).

In autonomous vehicles it is often applied as safety sensor, e. g. for the detection of a step or, in small robots, as a cheap sensor to explore the environment.

A triangulation sensor based on infrared was introduced by Sharp.[5] This sensor has a close-up range of 8–80 cm and delivers distance data with high precision and high resolution. In this sensor type the reflected light is projected onto a PSD or a 1D CCD-camera. The position x of the reflected light on the line camera with distance l to the infrared sender can directly be converted into the distance d to an obstacle with $d = f \cdot l/x$ (f is the focal length). Figure 3.18 shows the principle. The angular shift of ϵ between the focal plane of the lens and the CCD-line corrects for the shift in focal length for different distances. Figure 3.19 shows the principle of two reflective sensors for small distances.

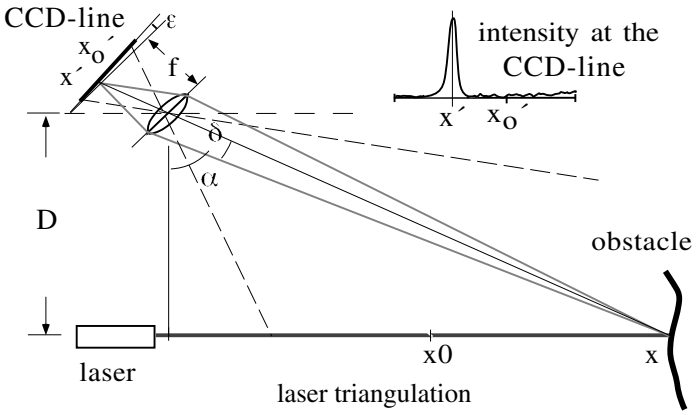

Figure 3.18 Measurement principle of an infrared triangulation sensor. x is the distance, f the focal length, D the distance between sender and linear camera and x' the intensity maximum in the linear camera picture.

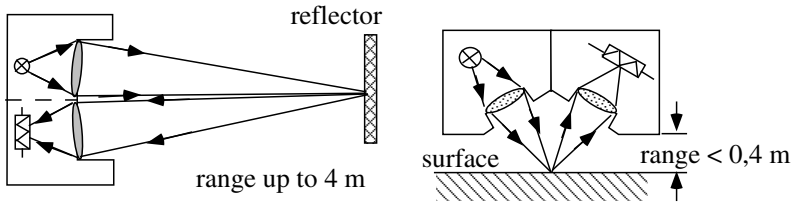

Figure 3.19 Reflexion light sensors; larger and short range

[5] http://www.sharpsme.com/Page.aspx/europe/en/

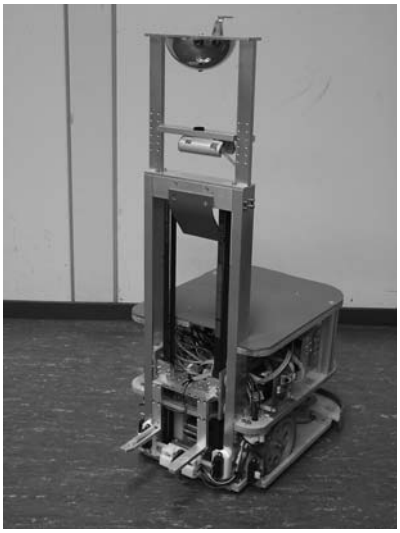

Figure 3.20 This forklift robot uses infrared sensors for collision avoidance.

3.4.2 Ultrasonic sensors

An ultrasound sensor bounces off a broad cone of ultrasound and measures an echo signal from obstacles in this cone. Ultrasonic sensors are often used as safety sensors in autonomous vehicles. To create ultrasound waves two principals are used: oscillating membranes and piezo crystals.

A thin metallic membrane of 50 mm diameter is electrostatically set into oscillations at a frequency around 50 kHz. The membrane sends out ultrasound pressure waves at a velocity of $c_{\text{us}} = 330\,\text{m/s}$ towards an obstacle. A reflected signal is picked up by the same membrane that is now used as a receiver. The time-of-flight is a measure for the distance to an object. In contrast to audible sound, ultrasound signals are attenuated severely in air, 11 m are the limit for 50 kHz signals. From the time t_L between start and first echo the distance is calculated as $L = c_{\text{us}} t_L/2$. The velocity of sound changes with temperature, air pressure and moisture content but may be treated as constant for the small distances of interest here. At 50 kHz the wavelength is $\lambda = 6{,}6\,\text{mm}$.

The other type of ultrasound sensor is based on a piezo crystal. A piezo crystal changes its width if a voltage is applied to both sides of a crystal plate or produces a voltage under compression. A Sick sensor[6] presented in figure 3.23 uses this principle.

[6] `http://www.sick.de/products/categories/industrial/ultrasonic/de/html`

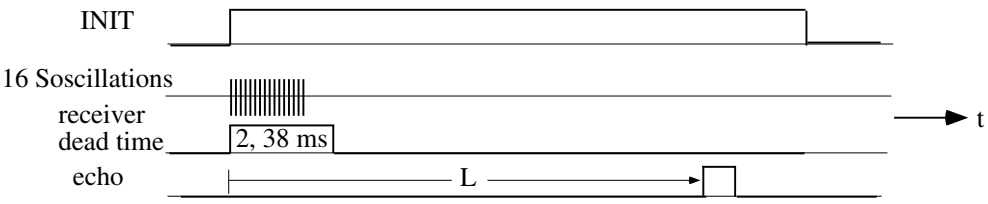

Figure 3.21 The operating principle of a emitter-receiver-module (Transducer) developed by Polaroid. After an initialization phase the polaroid sensor, with a membrane diameter 50 mm and a frequency of $f = 49.1$ kHz, sends out 16 oscillations in a cone angle of 30°. The time to the return of the reflected signal is measured. The measure range of the sensor is 20 cm–10.5 m with a resolution of 1%.

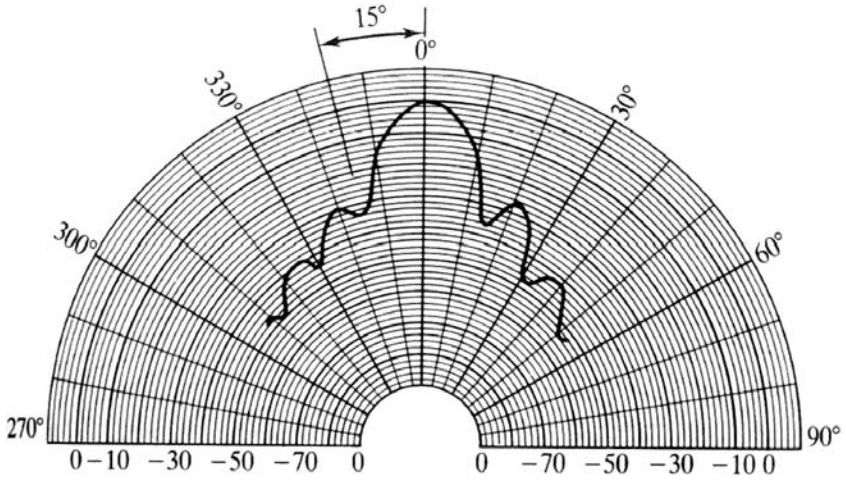

Figure 3.22 Cone of an ultrasound transceiver

Figure 3.23 Ultrasound sensor

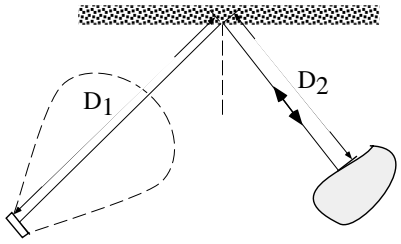

Figure 3.24 Hard surface reflecting like a mirror

Ultrasonic distance measurement also has disadvantages:

Surface roughness Any surface with a roughness that is small compared to the ultrasound wavelength used acts as a mirror, deflecting the sound without a return signal. For 50 kHz ultrasound any wall with surface roughness less than 5 mm behaves this way.

Multiple Reflections Misreadings are possible if the reflected signal hits an obstacle before it is bounced back to the sensor. In this case a distance much larger than the real one is calculated (in figure 3.24 $D_1 + D_2$ instead of D_1).

Soft materials Soft materials like pillows or curtains are strong ultrasound absorbers and can not be seen by the sensor.

Similar external signal An external ultrasound signal like pressurized air leaking into the environment could be misinterpreted if it has the same frequency range as the ultra sound sensor.

Crosstalk If more than one sender is firing simultaneously, the returning signals might overlap. This is called crosstalk.

3.4.3 Correlation of ultrasound signals

Some of the deficiencies occurring with ultrasonic measurements can be prevented by introducing correlation techniques [Joe98]. How similar are two given signals $x(t)$ and $y(t)$ to each other? The idea is to multiply the signals with a built-in time shift τ in one signal and integrate the product. The time shift is the characterizing parameter.

Crosscorrelation

$$P_{xy}(\tau) = \frac{1}{2T} \int_{-T}^{+T} x(t)y(t-\tau)dt \tag{3.5}$$

We see that a strong peak will occur whenever the signals are similar if shifted by a time τ_0 as shown in figure 3.25.

Autocorrelation

$$P_{xx}(\tau) = \frac{1}{2T} \int_{-T}^{+T} x(t)x(t-\tau)dt \tag{3.6}$$

This causes a peak whenever there are periods in a signal. For uncorrelated signals there is a single peak at $\tau = 0$, as shown in figure 3.26. Signals in the form of broadband noise have small crosscorrelation and good autocorrelation, as shown in figure 3.27.

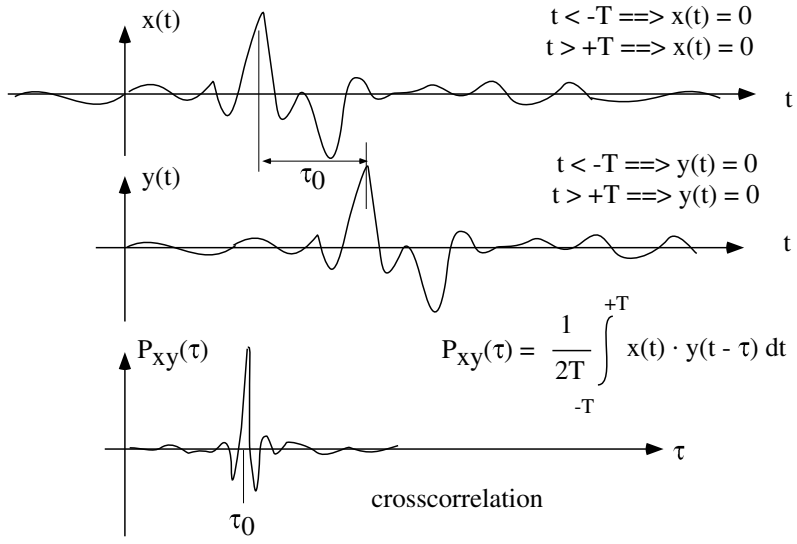

Figure 3.25 Crosscorrelation

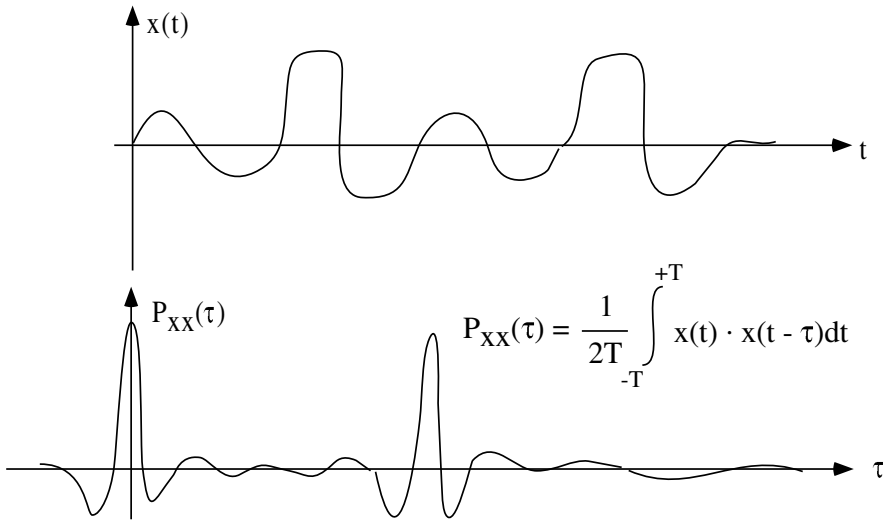

Figure 3.26 Autocorrelation

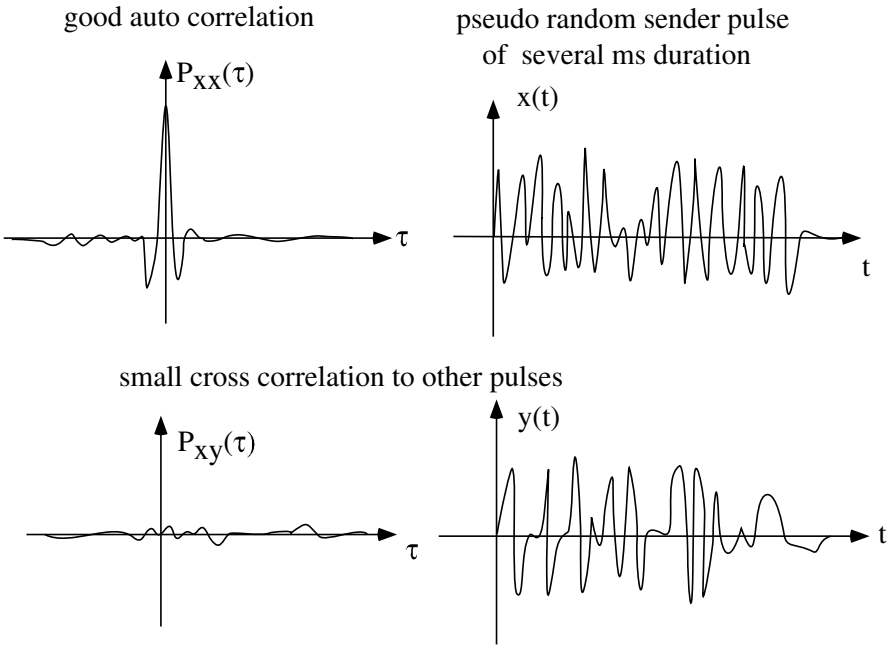

Figure 3.27 Pseudo random pulse

The correlation of signals $x(t)$ and $y(t-\tau)$ may be calculated using Fourier transforms:

$$P_{xy}(\tau) = \frac{1}{2\pi} \int_{-\infty}^{+\infty} F^*(\omega) \cdot G(\omega) e^{-i\omega\tau} d\tau \tag{3.7}$$

$$F^*(\omega) = \int_{-\infty}^{\infty} x(t) \cdot e^{-i\omega t} dt \tag{3.8}$$

$$G(\omega) = \int_{-\infty}^{+\infty} y(t-\tau) e^{i\omega t} dt \tag{3.9}$$

Let $x(t) = 0$ and $y(t) = 0$ for $t < 0$ and $t \geq N \cdot \Delta t$ denote two signals. Discretizing $x(t) \longrightarrow [x_j]$ and $y(t) \longrightarrow [y_j]$ under the discretization $x_j = x(j \cdot \Delta t)$ allows us to calculate the Fast Fourier Transforms (FFT) $F(\omega) \longrightarrow [F_k]$ and $G(\omega) \longrightarrow [G_k]$.

$$F_k^* = \sum_{j=0}^{N-1} x_j \cdot e^{-i2\pi jk/N} \tag{3.10}$$

$$G_k = \sum_{j=0}^{N-1} y_j \cdot e^{i2\pi jk/N} \tag{3.11}$$

where $j,k = 0,\ldots,N-1$ and $N = 2^n$. The back transformation delivers $P_{xy}(\tau) \longrightarrow [P_{xy}(\tau_m)]$ with $\tau_m = m \cdot \Delta t$

$$P_{xy}(\tau_m) = \frac{1}{2\pi} \sum_{j=0}^{N-1} F_k^* \cdot G_k e^{-i2\pi mk/N} \tag{3.12}$$

Using suitable pseudo random signals of 10 ms duration correlating the transmitted and received impulses allows a precise measurement of distances despite crosstalk. Two objects nearby each other may be discriminated as shown in figure 3.28.

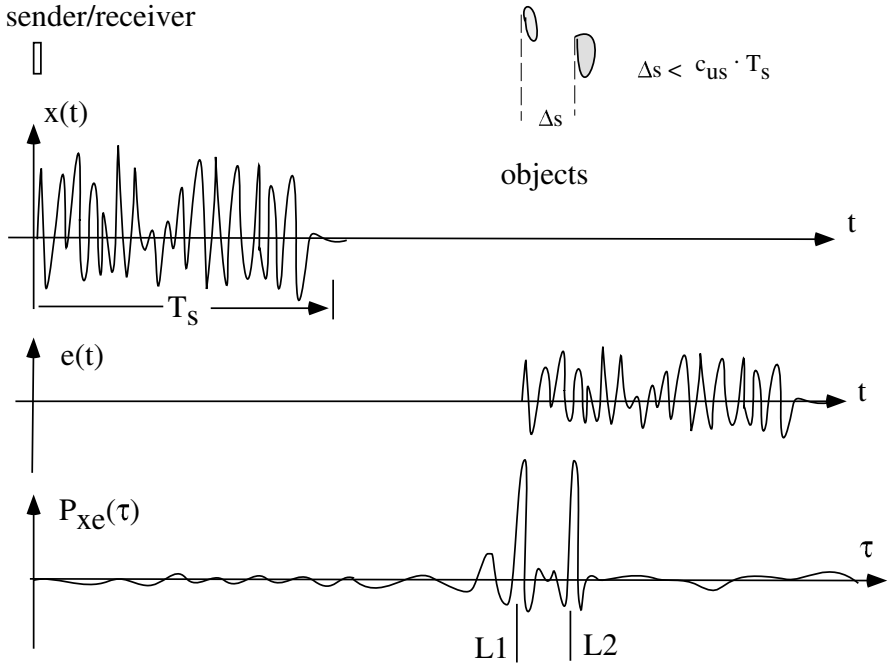

Figure 3.28 Better distance resolution

3.4.4 Laser sensors

Laser radar sensor The most prominent sensor of this type is the Sick PLS sensor.[7] It is an active laser sensor operating on narrow pulses of 1 ns length but 10 W power with 4500 pulses/s (eye safe) in the near infrared section of

[7] Sick Optoelectronic Waldkirch, Baden, Germany; `http://www.sick.de/de/products/categories/safety/de.html`

the spectrum. On emission of a pulse, a fast counter is started and stopped again at the first return of a signal, picked up by a rather large mirror and an avalanche photo diode. The counter directly measures the distance to an obstacle. Within 1 ns the light travels 15 cm from the sender towards an obstacle and the same distance back again towards the receiver. Figure 3.29 illustrates this principle.

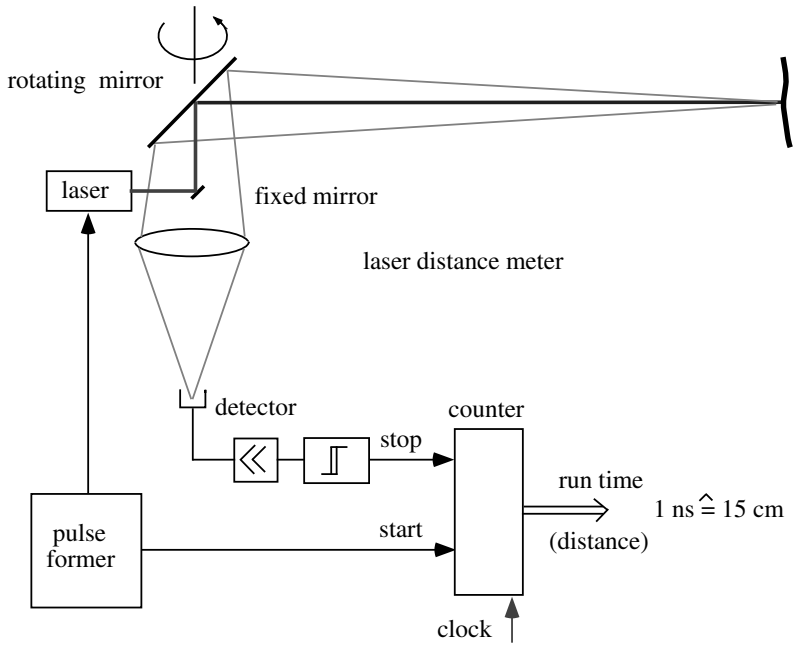

Figure 3.29 Principle of the Sick laser scanner

Each tick of the counter denotes a distance of 5 cm. As the emitted signal is rather strong, every surface with a reflectivity larger than 1.8% (black leather, dust on a polished glass surface or a fly in the beam) gives enough reflection to see a return signal and detect an obstacle. The scanning range of the sensor is 180°. 361 measured distances taken every 0,5° form a laser scan (running period 80 ms). Further information is printed in the table below. The sensor is licensed in the EU to be used to trigger an emergency stop for distances less than 4 m. Figure 3.30 shows a picture of the sensor.[8] Figure 3.31 shows a laser radar scan of a room with some furniture in it; the grid width is 1 m.

[8] `http://www.sick.de/`

The main parameters of a Sick laser range sensor are listed below:

Cone angle	180°
Angle resolution	1°/**0.5°** / 0.25°
Response time	13 ms / **26 ms** / 53 ms
Resolution	10 mm
Systematic error	±15 mm
Statical error at 1 σ	5 mm
Measurement range	8 m, 16 m, 32 m, **80 m**
Transfer rate	9.6/19.2/38.4/**500** kBaud
Working temperature	0...+50°C
Supply voltage	24 V ±15%
Weight	ca. 4.5 kg
Size (H × L × W)	210 mm × 156 mm × 155 mm

Figure 3.30 The Sick laser scanner LMS200

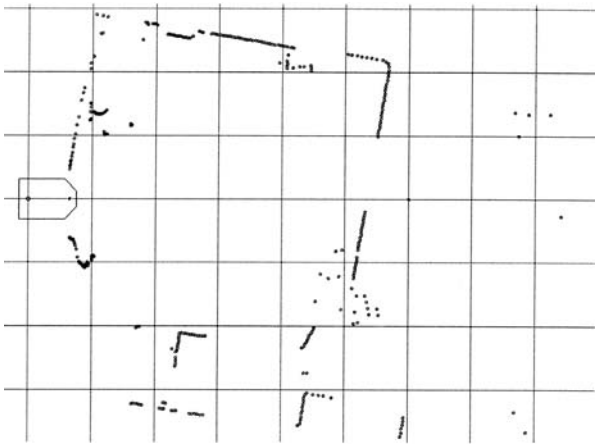

Figure 3.31 Typical laser scan of a room

3.5 Vision sensors

There are two important semiconductor sensors available for computer vision: CCD and CMOS. The basis of semiconductor cameras is the "inner photoelectric effect": In certain materials electrons are set free under photon absorption (light). The amount of electrons is correlated to the amount of photons. While CMOS sensors offer small size, bigger dynamics and show no blooming effects, the CCD sensor has higher photo sensitivity, higher uniformity and less noise.

3.5.1 CCD camera

CCD chips are sensitive to the complete visible spectrum, but especially to red light. Color images are created through application of RGB filters and a combination of 4 photo diodes for 1 pixel. One problem with CCD technology is the evaluation per column. Under intense light this leads to the so-called "blooming" where a column seems to be fully illuminated. During integration of charges the pool may be flooded. This effect can be avoided with "drain canals" on the chip, reduction of exposure time or reduction of shutter opening time.

3.5.2 CMOS camera

CMOS technology offers a continuous conversion of the photon beam into output voltage while each cell or pixel can be accessed directly. Therefore, CMOS is more expensive than CCD.

3.5.3 Stereo-camera systems

Binocular stereo vision Humans are able to perceive depth information with their two eyes. A distant object is projected onto the retina of the left and right eye. The object's projections differ in their position. The human brain is able to generate a depth judgment for that object by analyzing the two images.

Computer stereo vision copies this concept. The goal is to reconstruct a depth map from at least two 2D camera images showing a 3D scene from different observation points. The depth information can be inferred by matching a point in both images and looking at the displacement between the matched

pair. Figure 3.32 visualizes the general case of stereo vision geometry with two input images.

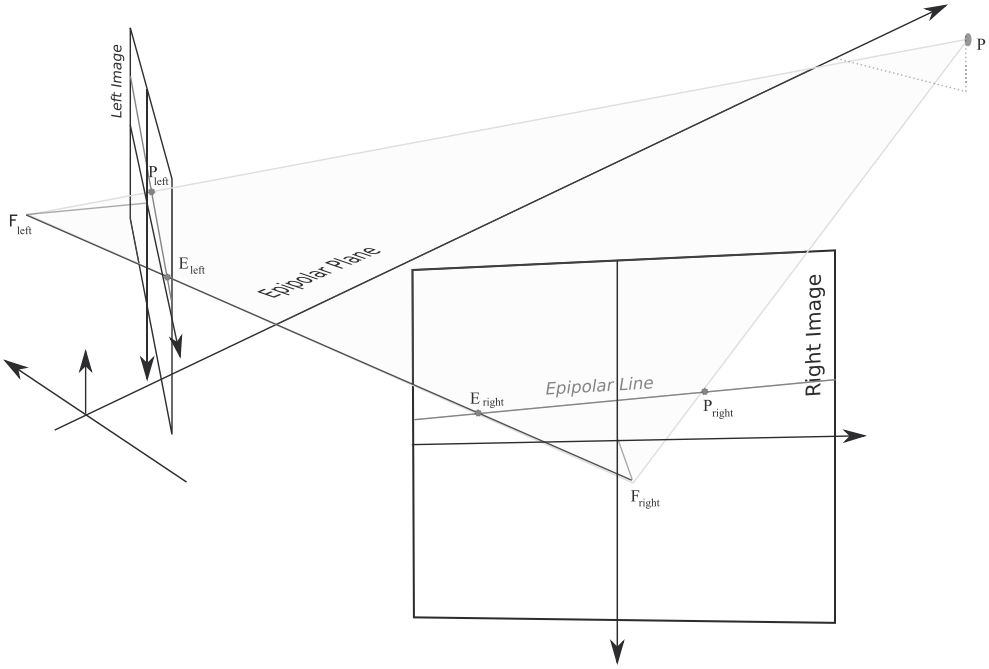

Figure 3.32 General stereo vision geometry (pin-hole camera model). E_{left}, E_{right}: epipolar points; F_{left}, F_{right}: focal points; P: point in 3D space; P_{left}, P_{right}: projections on image planes

A 3D scene is projected onto two 2D virtual image planes. The plane defined by point P and both focal points F_{left} and F_{right} is called *epipolar plane*.

The projected line from focal point F_{left} to P in the right image is called an *epipolar line*. The right image projection P_{right} of point P can always be found on this epipolar line. This is called the *epipolar constraint* and simplifies the correspondence problem. This constraint only holds for the perfectly rectified images of a pin-hole camera. In reality, raw camera images are usually distorted. The images have to be rectified prior to stereo vision processing.

A binocular stereo vision system with *canonical stereo geometry* consists of two identical cameras mounted in parallel. The cameras are placed so that their virtual image planes and both epipolar lines fall together (see figure 3.33). The epipolar lines are aligned parallel to the x-axis of the image planes.

Each point in the observed scene will be projected to the same row in the left and right image but on different pixels here. The displacement between left and right projection is called *disparity* d.

In order to reconstruct the 3D scene from disparity values, the fixed distance between the cameras called *baseline* b and the focal length f of the cameras has to be known.

The stereo vision head coordinate system lies between both cameras on the baseline. Its orientation is defined according to common decisions in robotics as a right-hand coordinate system. The x-axis pierces perpendicular through the image plane (see figure 3.33).

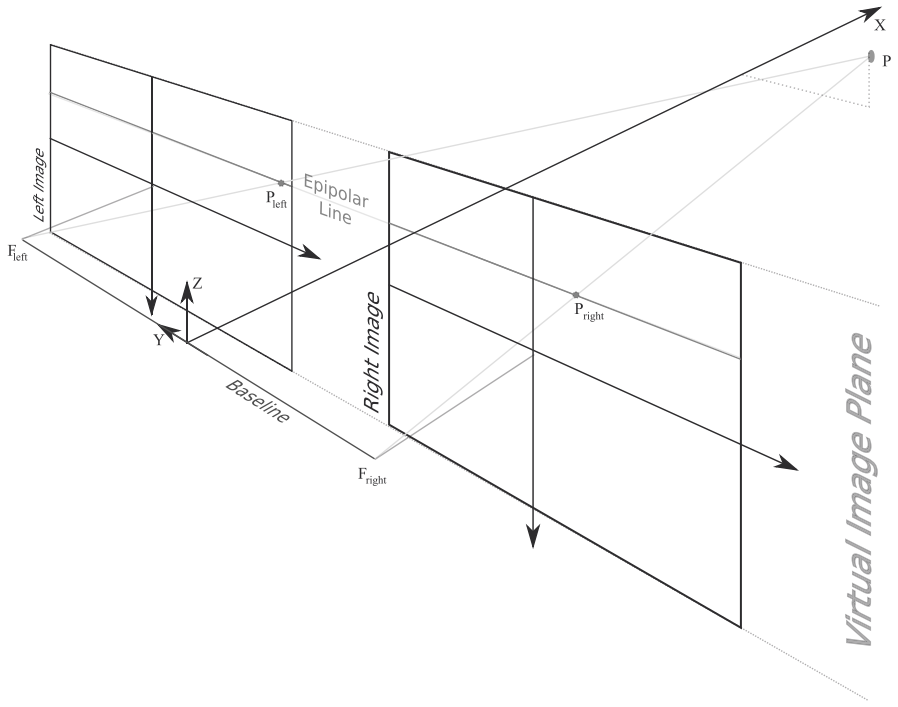

Figure 3.33 Binocular stereo vision setup

In computer vision, the origin of an image usually lies in its top left corner. Here, the image coordinate systems have their origins translated to the very middle of each picture, closest to the focal point (see figure 3.33). This is not a restriction. It only simplifies the following derivation and is a common assumption in physics for the pin-hole camera model.

The exact 3D coordinates x, y and z for two matching pixel (x_l,y_l) and (x_r,y_r) can be calculated using triangulation as shown in figure 3.34.

$$\tan(\alpha_l) = \frac{x_l}{f} = \frac{\frac{b}{2} - y}{x} \tag{3.13}$$

$$\tan(\alpha_r) = \frac{-x_r}{f} = \frac{\frac{b}{2} + y}{x} \tag{3.14}$$

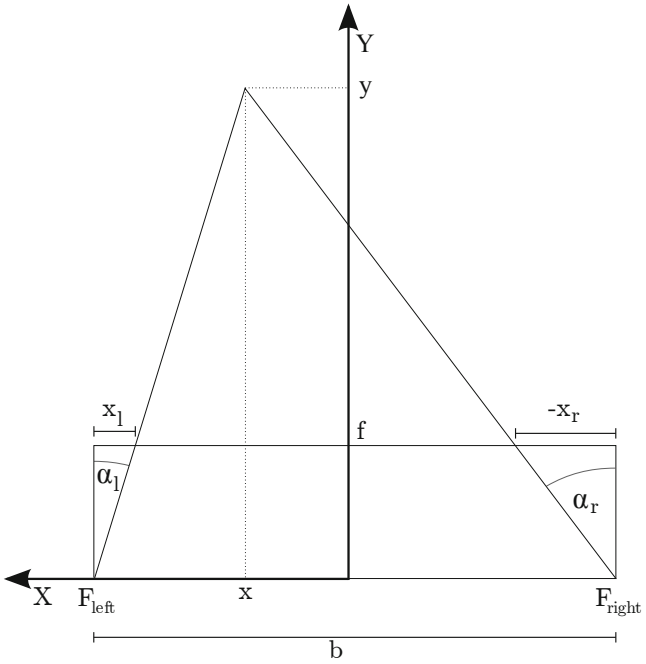

Figure 3.34 X-y-plane triangulation (top view on stereo vision head)

Solving 3.13 and 3.14 for y yields:

$$y = \frac{-x_l \cdot x}{f} + \frac{b}{2} \tag{3.15}$$

$$y = \frac{-x_r \cdot x}{f} - \frac{b}{2} \tag{3.16}$$

Equating 3.15 and 3.16 and solving for x results in:

$$x = \frac{b \cdot f}{x_l - x_r} \tag{3.17}$$

Solving for z is even simpler. Since both pixels lie on the same image row $y_r = y_l$ holds, see figure 3.35.

$$\tan(\beta) = \frac{y_l}{f} = \frac{z}{x} \tag{3.18}$$

$$z = \frac{x \cdot y_l}{f} \tag{3.19}$$

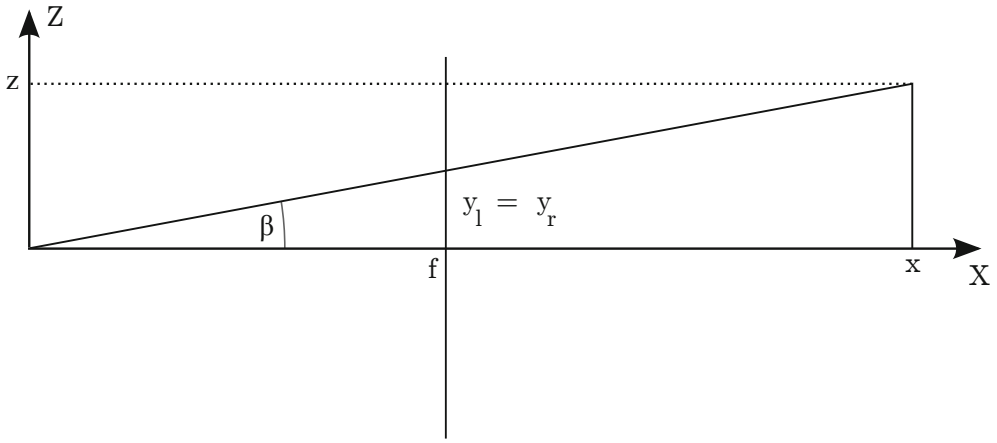

Figure 3.35 X-z-plane triangulation (side view on stereo vision head)

Substitution of equation 3.17 into 3.19 and 3.15 yields the following formulas for straight forward computation of y and z.

$$y = \frac{-\frac{b}{2} \cdot (x_l + x_r)}{x_l - x_r} \tag{3.20}$$

$$z = \frac{y_l \cdot b}{x_l - x_r} \tag{3.21}$$

The disparity value d calculated by a stereo vision algorithm already equals $x_l - x_r$. Note that the translation of the image origin along the x-axis has no effect on the disparity. Let the left image be the reference image. Then x_l and d are known. x_r can easily be calculated as $x_r = x_l - d$.

Stereovision algorithms The challenge for a stereo vision algorithm is to solve the correspondence problem, i. e. finding the right match in the left and right image for a given point in the real world. The common approach is to declare one input image as the reference image. For a pixel in the reference image the corresponding pixel is then searched for in the second input image.

However, finding the correct match is ambiguous. Due to occlusion some points may not have a match in the other projection (see figure 3.36). Furthermore, repetitive textures may produce multiple matches. Detecting occlusion and finding the right match determines the quality of a stereo vision algorithm.

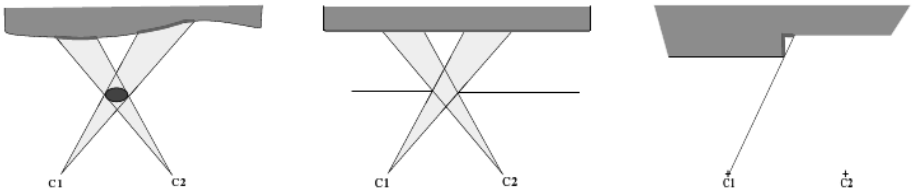

(a) (b) (c)

Figure 3.36 Scene configurations with half-occluded regions (highlighted in red): (a) occlusions due to thin object at the foreground-scene discontinuity, (b) occlusion due to a small hole at the foreground-scene discontinuity, (c) occlusion due to surface variation-surface discontinuity (source [Kos02]).

Stereo vision strategies can be dense or sparse. Sparse stereo vision concentrates on selected feature points only. A feature point can be a point of special interest. Alternatively, a feature point may be a point with high likelihood for a good match. This approach can potentially result in a fast stereo vision algorithm due to the reduced amount of analyzed points. Dense stereo vision algorithms find matches for all points in the reference image (a dense approach was chosen here since distance information for the whole image is required for further processing steps). In a complete run of a dense stereo vision algorithm, a disparity value is calculated for each pixel in the reference image. Typically this result is visualized as a gray scale image, also known as disparity map. In this image each pixel's brightness corresponds to a disparity level. High disparity values result in lighter pixels.

Instead of finding suitable feature points in a pre-processing step, the disparities for all pixels are computed in parallel. Therefore, points with high confidence can serve as sparse feature points if needed.

Global vs. window-based optimization Recently, high quality results have been achieved in CPU stereo vision by applying global optimization techniques to the stereo vision problem (see [SS02]). Such algorithms rank top at the Middlebury evaluation page.[9] However, these approaches tend to be slow and thus are not suitable for our near-real-time task. Yang and Pollefeys [YP05] claim that only correlation-based stereo algorithms can provide

[9] `http://vision.middlebury.edu/stereo/`

a dense depth map in real time on standard computer hardware. However, a fast optimizing stereo vision algorithm for the GPU could be an interesting future research topic.

GPU computation profits from parallelizing, while inter-process communication is extremely limited[10] or expensive[11]. In this work a window-based approach was chosen.

Window-based stereo algorithms take two parameters: window width and window height. The window describes a rectangle area around the reference pixel. Around a match candidate in the second image a rectangle of equal size is compared to the reference window, see figure 3.37. The most similar areas are taken to be the correct match.

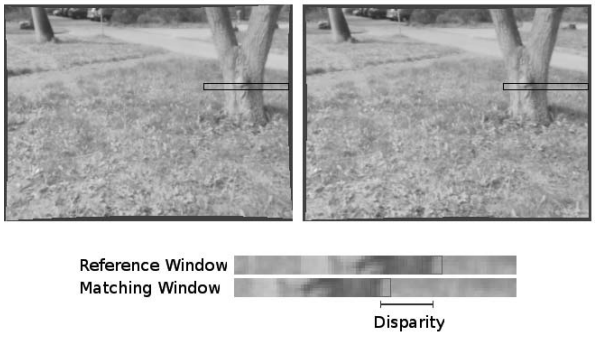

Figure 3.37 Window-based stereo vision

For each disparity step a window-based strategy shifts the window along the epipolar line in the second image. The region in both images is then compared by a similarity function. The disparity step with the highest similarity most likely provides the correct match. Common similarity functions are cross correlation, sum of squared differences (SSD) or sum of absolute differences (SAD).

The performance and quality of a window-based algorithm depends on the window size. Large support regions provide a higher certainty for a correct match even for low textured input images. Small window sizes speed up the computation and produce finer grained results. Window-based stereo vision requires good textures in the input images. Luckily, in the application field of outdoor robotics such textures prevail.

[10] shared memory accessible for threads in same block only
[11] global memory access is slow